New Journal of Physics
The open access journal at the forefront of physics

Deutsche Physikalische Gesellschaft DPG IOP Institute of Physics

FAST TRACK COMMUNICATION • OPEN ACCESS

Determination of CaOH and $CaOCH_3$ vibrational branching ratios for direct laser cooling and trapping

To cite this article: Ivan Kozyryev *et al* 2019 *New J. Phys.* **21** 052002

New Journal of Physics
The open access journal at the forefront of physics

Deutsche Physikalische Gesellschaft DPG
IOP Institute of Physics

Published in partnership with: Deutsche Physikalische Gesellschaft and the Institute of Physics

OPEN ACCESS

RECEIVED
14 December 2018

REVISED
25 March 2019

ACCEPTED FOR PUBLICATION
16 April 2019

PUBLISHED
8 May 2019

FAST TRACK COMMUNICATION

Determination of CaOH and $CaOCH_3$ vibrational branching ratios for direct laser cooling and trapping

Ivan Kozyryev[1,2,4,5], **Timothy C Steimle**[3,5], **Phelan Yu**[1,2], **Duc-Trung Nguyen**[3] and **John M Doyle**[1,2]

[1] Harvard-MIT Center for Ultracold Atoms, Cambridge, MA 02138, United States of America
[2] Department of Physics, Harvard University, Cambridge, MA 02138, United States of America
[3] School of Molecular Sciences, Arizona State University, Tempe, AZ 85287, United States of America
[4] Present address: Department of Physics, Columbia University, New York, NY 10027, United States of America.
[5] Author to whom any correspondence should be addressed.

E-mail: ivan@cua.harvard.edu **and** tsteimle@asu.edu

Keywords: laser cooling, polyatomic molecules, multidimensional Franck–Condon factors, dispersed laser-induced fluorescence

Abstract

Alkaline earth monoalkoxide free radicals (MORs) have molecular properties conducive to direct laser cooling to sub-millikelvin temperatures. Using dispersed laser induced fluorescence measurements from a pulsed supersonic molecular beam source we determine vibrational branching ratios and Franck–Condon factors for the MORs CaOH and $CaOCH_3$. With narrow linewidth continuous-wave dye laser excitation, we precisely measure fluorescence branching for both $\tilde{X}$–$\tilde{A}$ and $\tilde{X}$–$\tilde{B}$ electronic systems in each molecule. Weak symmetry-forbidden decays to excited bending states with non-zero vibrational angular momentum are observed. Normal mode theoretical analysis combined with *ab initio* structural calculations are performed and compared to experimental results. Our measurements and analysis pave the way for direct laser cooling of these (and other) complex nonlinear polyatomic molecules. We also describe a possible approach to laser cooling and trapping of molecules with fewer symmetries like chiral species.

1. Introduction

Detailed quantum mechanical understanding of dynamics, interactions, and reactions for complex molecules requires precisely targeted preparation of internal molecular states and relative kinetic motions in the gas-phase solvent-free environment [1–3]. Supersonic molecular beams have allowed groundbreaking achievements in experimental studies of inelastic and reactive molecular interactions, as well as opened the path to coherent control of internal molecular states [4–9]. With some crucial exceptions, however, large velocity in the laboratory frame usually leads to short experimental coherence times and averaging over multiple internal and motional quantum states. The emergence of cryogenic buffer-gas beams (CBGBs) led to a significant reduction in the forward velocity but the highest molecular fluxes still maintained $\gtrsim$10 K kinetic energy in the laboratory frame [10]. Therefore, other experimental techniques have emerged in particular those aimed at reducing the forward velocity of molecular beams to the degree sufficient for eventual three-dimensional confinement inside conservative electromagnetic traps, enabling seconds-long coherence times [11]. Molecular trapping also opens opportunities for accurate collisional studies at very low temperatures.

The use of electric, magnetic, optical and mechanical techniques for molecular beam slowing have all been experimentally demonstrated, with published comprehensive reviews providing excellent survey of the field [11, 12]. Recent advances in direct molecular cooling as well as coherent molecule formation from unbound atoms have led to the emergence and rapid development of a new vibrant field of cold and ultracold chemistry [3, 13]. The unprecedented opportunity to completely control the internal molecular degrees of freedom, as well as external motion, of diverse molecular species has yielded exciting observations on the role of quantum statistics in molecular reactive collisions as well as confining geometry of the reactants, among other results [3].

However, with few crucial exceptions [6, 9, 14, 15], the studies have been limited to the exploration of diatomic molecules which can be prepared from associated laser-cooled atomic samples.

Extension of the available experimental techniques to production of a chemically diverse set of polyatomic molecules will aid in benchmarking state-of-the-art *ab initio* calculations as well as shed light on novel reaction mechanisms at work. Given the recent rapid experimental progress on laser cooling and trapping of diatomic molecules [16–20], we consider the extension of these techniques to polyatomic species. The internal quantum complexity of polyatomic molecules grows significantly upon transitioning from polar diatomic radicals with a single vibrational mode to nonlinear polyatomic molecules with multiple rotational and vibrational degrees of freedom. Nevertheless, a large number of different monovalent alkaline earth derivatives have been proposed to be amenable to laser cooling [21, 22], with pioneering experimental work on the laser-cooling of the triatomic SrOH molecule [23].

In polyatomic molecules, the absence of strict angular momentum selection rules for transitions between totally symmetric vibrational modes presents a new challenge for photon cycling [24], a necessary ingredient for laser cooling. Additionally, higher-order perturbation mechanisms present only in polyatomic molecules such as Fermi resonance as well as Jahn–Teller and Renner–Teller interactions can lead to Born–Oppenheimer breakdown and coupling between vibrational modes, which can result in loss channels otherwise forbidden by the symmetries of the original unperturbed states. Spin-rotation and hyperfine splittings are in the MHz regime and can be efficiently addressed by adding radio-frequency sidebands to the cycling laser; rotational splittings are in the GHz range and can be coupled to the 'bright' rotational state with microwaves; however, vibrational transitions are in the THz range and would require additional laser systems, significantly increasing experimental complexity. Thus, precise measurements of Franck–Condon factors (FCFs) and vibrational branching ratios (VBRs) are crucial in determining the experimental feasibility of laser cooling.

While there is plenty of theoretical work on the estimation of FCFs and VBRs for both diatomic [25–27] and polyatomic molecules [21, 22, 28], accurate experimental studies have been limited primarily to diatomic species [29–32] and, recently, SrOH [33]. Accurate theoretical predictions of FCFs for polyatomic molecules remain a challenge because their multidimensional nature not only introduces interactions between the degrees of freedom on each potential surface but also between the coordinates of the two electronic states. The pair of molecules we have chosen to study here represent the simplest (by geometric structure) members of the alkaline earth monoalkoxide radicals (MOR) family [34, 35], a large class of polyatomic molecules that has previously been proposed for laser cooling applications [21]. A simple 'triatomic' model of the MOR molecules has been used in order to estimate branching ratios and indicated that laser cooling of relatively large MOR molecules with up to 15 constituent atoms could be possible. Our precise measurements of VBRs for CaOH and $CaOCH_3$ described below provide the first experimental validation of the theoretical model of 'shielding' of the R ligand group (e.g. CH_3) vibrational modes by the intermediate oxygen atom [21]. Increased density of vibrational states for larger polyatomic molecules could potentially lead to internal vibrational redistribution among multiple vibrational normal modes leading to enhanced loss probabilities and, therefore, necessitating accurate experimental studies.

CaOH is one of the first polyatomic molecules to be proposed suitable for laser cooling and trapping and detailed theoretical *ab initio* calculations have been performed of the FCFs [22] as well as energy levels [36]. Our work provides an important comparison between the theoretical and experimental results, benchmarking theoretical calculations by Isaev and Berger [22]. Our precise measurements of the branching ratios for a more complex symmetric-top molecule (STM) $CaOCH_3$ provide, to the best of our knowledge, the first accurate experimental study of the VBRs for a nonlinear radical suitable for direct laser cooling. Particularly, our results indicate the necessity to consider pseudo Jahn–Teller couplings in the excited electronic levels of polyatomic molecules [37]. Perhaps surprisingly, despite the presence of Jahn–Teller interaction in the electronically degenerate E symmetry state of the C_{3v} symmetric top, using the lowest allowed $\tilde{X}^2A_1 \leftrightarrow \tilde{A}^2E_{1/2}$ electronic excitation will lead to ~16 scattered photons without any additional repumping lasers. Based on our experimental measurements and theoretical analysis, we propose a feasible route for producing large ultracold samples (~10^3–10^6 molecules) of both radicals via laser cooling on the lower spin–orbit (SO) branch of the $\tilde{X}$–$\tilde{A}$ electronic transition. Performing a detailed study of inelastic and reactive collisions on increasingly complex members of the CaOR molecule family would provide a unique window into the scattering properties of fundamental ligand groups in organic chemistry.

2. Experimental configuration

Since the details of the experimental apparatus have previously been described in other publications [33], we provide only a brief account of the experimental configuration employed. As a source of cold molecules we used a pulsed supersonic molecular beam with argon as a carrier gas. Both CaOH and $CaOCH_3$ beams were created by

flowing argon over a container filled with liquid methanol (CH_3OH) maintained at room temperature. Room temperature vapor pressure of methanol (~10 kPa) together with the backing pressure of argon (~4000 kPa) was enough to seed a sufficient number of gas-phase molecules into the carrier gas to observe large, stable yields of both molecular radicals of interest following laser ablation of a calcium metal target. The peak fluorescence signal per single rovibrational level was approximately of similar magnitude for CaOH and $CaOCH_3$, which allowed for accurate studies of both radicals using the same beam source. Molecules in a specific rotational state were excited using a single frequency cw-dye laser. Dispersed fluorescence data was collected with a spectrometer that included 0.67 m focal length, high-efficiency Czerny–Turner-type monochromator with a low-dispersion grating and a cooled, gated intensified charge-coupled device camera. The relative sensitivity as a function of wavelength for the spectrometer was precisely calibrated beforehand. The wavelength resolution of the emission spectrum was controlled by adjusting the width of the monochromator input aperture and absolute calibration was performed with the argon emission lamp. The measured emission wavelengths agreed to $\lesssim$0.1 nm with theoretical predictions which allowed for unambiguous identification of the vibrational loss channels. The narrow linewidth ($\lesssim$1 MHz) of the excitation dye laser allowed accurate rotationally-resolved excitation. A Burleigh high-resolution wavemeter was used as a rough frequency reference (<1 GHz), additionally confirmed by co-recording with some Doppler I_2 spectrum [38]. For each dispersed laser induced fluorescence (DLIF) measurement, three separate datasets were taken: (i) signal dataset with ablation Nd:YAG laser on and dye laser on, (ii) scattered background dataset with no Nd:YAG laser but dye laser on, and (iii) spurious ablation glow dataset with Nd:YAG laser present but no dye laser. The resulting measurement was obtained by subtracting datasets (ii) and (iii) from (i) in order to remove the scattered light offset and reduce the background ablation glow (e.g. metastable calcium emission).

3. Experimental determination of branching ratios

In order to eliminate rotational branching during the photon cycling process the use of $J'' \rightarrow J' - 1$ type angular momentum transitions has been proposed [39, 40] and for the first time demonstrated with diatomic SrF in [41] and linear triatomic SrOH in [42]. Rotationally-resolved high-resolution spectroscopy of low-J rotational levels of CaOH and $CaOCH_3$ has been previously performed and assigned for both $\tilde{X}$–$\tilde{A}$ and $\tilde{X}$–$\tilde{B}$ electronic bands [43–49]. The availability of prior spectroscopic measurements, low rotational temperatures of the skimmed supersonic molecular beam as well as the narrow linewidth of the cw dye laser, allowed us to deliberately address only the rotational transitions which can be used for optical cycling and laser cooling. Additionally, the absence of state-changing collisions in the probing region eliminated any possible systematic errors.

While both CaOH and $CaOCH_3$ have spin-rotation and hyperfine splittings arising from the unpaired electron and hydrogen spins, correspondingly, for the purposes of the experiments performed here we label the states using rotational quantum numbers $|N,\ K\rangle$ for non-degenerate quantum states (i.e. Σ^+ states for linear molecules and A_1 states for STMs) and $|J,\ K\rangle$ states for degenerate states (i.e. Π electronic states for linear molecules and E states for STMs) with $K = 0$ for linear molecules. Upon the electronic excitation to a specific rotational level, the spontaneous emission rate for a dipole-allowed transition is governed by the Einstein A coefficient [50]:

$$A_{J' \rightarrow J''} = \frac{16\pi^3 \nu^3 S_{J'J''}}{3\epsilon_0 hc^3 (2J' + 1)}, \tag{1}$$

where the molecular line strength $S_{J'J''} \equiv \sum_{M',M''} |\langle J'M'|\boldsymbol{\mu}|\ J''M''\rangle|^2$ is approximately given as

$$S_{J'J''} = q_{\mathbf{v}'-\mathbf{v}''} |\mathbf{R}_e|^2 S_{J''}^{\Delta J} \tag{2}$$

under the Born–Oppenheimer separation $\psi_{\rm tot} = \psi_{\rm el}\psi_{\rm vib}\psi_{\rm rot}$. Therefore, the intensity of different vibrational bands will be proportional to

$$\mathrm{VBR} = \frac{\nu^3 q_{\mathbf{v}'-\mathbf{v}''}}{\sum_i \nu_i^3 q_{\mathbf{v}'-\mathbf{v}''}} \tag{3}$$

since the same electronic transition dipole moment $|\mathbf{R}_e|$ and Hönl–London rotational factor are shared by all the vibronic emission bands. Additionally, the rotational branching is limited by the $\Delta J = 0, \pm 1$ selection rule and all J branches contribute identically for all the vibrational bands. For polyatomic molecules, the FCF is multidimensional and given as

$$q_{\mathbf{v}'-\mathbf{v}''} = q_{v_1'-v_1''} q_{v_2'-v_2''} \ldots = \left| \int \psi_{v_1'}^* \psi_{v_1''} \mathrm{d}Q_1 \right|^2 \left| \int \psi_{v_2'}^* \psi_{v_2''} \mathrm{d}Q_2 \right|^2 \ldots \tag{4}$$

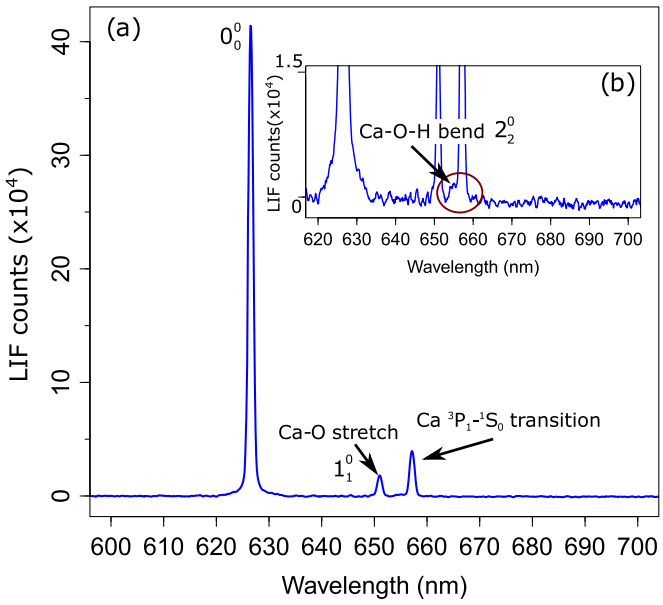

Figure 1. Measured CaOH vibrational branching in the $\tilde{X}$–$\tilde{A}$ electronic system. (a) Dispersed laser-induced fluorescence for CaOH excited on the $P_1(N'' = 1)$ branch of the $\tilde{X}^2\Sigma^+(000) \rightarrow \tilde{A}^2\Pi_{1/2}(000)$ transition at 626 nm. 4.3% ± 0.2% of the molecules decay to the first excited level of Ca–O stretching mode. The peak at 657 nm is due to spontaneous emission on the intercombination $^3P_1 \rightarrow {}^1S_0$ line of metastable calcium atoms created during the laser ablation process. (b) Zoomed in region of the plot indicating that all other decay channels are below 0.3%.

By comparing the integrated areas under the dispersed fluorescence emission peaks, we can determine the relative branching ratios for decays from a given electronic, vibrational and rotational state.

3.1. CaOH measurements

Two electronic transitions have been studied for CaOH that have potential to be used in the laser cooling and trapping applications. Previously, laser cooling of the isoelectronic CaF and SrOH molecules has been demonstrated using either the $\tilde{X}^2\Sigma^+$–$\tilde{A}^2\Pi_{1/2}$ or $\tilde{X}^2\Sigma^+$–$\tilde{B}^2\Sigma^+$ electronic transition and, therefore, we have performed detailed measurements on both bands for CaOH as well. Additionally, in order to increase the photon cycling rate it is favorable to avoid coupling multiple excitation lasers to the same vibronic level, thus requiring separation of the main cycling and repumping lasers to address different electronic levels (e.g. main cycling on $\tilde{X}$–$\tilde{A}$ while repumping on $\tilde{X}$–$\tilde{B}$ or vise versa). As was previously demonstrated both theoretically [51] and experimentally [52], when multiple ground state sub-levels n_{vg} from different vibrational levels v are coupled to the same excited state sub-levels n_{0e}, the effective scattering rate for molecules is reduced by a factor of $2n_{0e}/(n_{0e} + \sum_v n_{vg})$, resulting in a lower radiation pressure force ($F_{\rm rad}$). Therefore, the scattering rate and $F_{\rm rad}$ is maximized for decoupling all repumpers from the main cycling laser, resulting in a maximal possible scattering rate of $R_{\rm scat,max} = \Gamma_{\rm sp} n_{0e}/(n_{0e} + n_{0g})$, where $\Gamma_{\rm sp} = 1/\tau_{\rm sp}$ and $\tau_{\rm sp}$ is the spontaneous lifetime of the excited electronic state.

Figures 1 and 2 display the results of the DLIF for CaOH excited using the $P_1(N'' = 1)$ transition on the $\tilde{X}$–$\tilde{A}^2\Pi_{1/2}$ (at 15 964.38 cm^{-1}) and $\tilde{X}$–$\tilde{B}$ (at 18 021.58 cm^{-1}) bands, correspondingly. Similarly to the previous measurements with isoelectronic diatomic CaF [53] and triatomic SrOH [33], the intensity of the off-diagonal vibrational bands decreases rapidly, indicating the suitability of using either electronic transition for optical cycling. High sensitivity of our measurement allowed us to observe very weak decays to (02^00) and (01^10) excited bending vibrational states as shown in figures 1(b) and 2(b). Symmetry forbidden $\Delta l \neq 0$ vibronic decays in alkaline earth monohydroxides occur in second order due to $H_{\rm RT} \times H_{\rm SO}$ Hamiltonian term. The dipolar term of the Renner–Teller (RT) perturbation operator connects basis functions with $v_2 = \pm 1$ and $\Delta l = -\Delta\Lambda = \pm 1$ [54, 55] and together with the off-diagonal parts of the SO operator leads to coupling between $\tilde{B}(000) \sim \tilde{B}(01^10)$ states [56]. Decay to the (02^00) vibrational state is symmetry allowed and observed in our measurements (figure 1(b)), but the more precise determination of this band's intensity is limited by the contamination signal arising due to the 657 nm emission from the metastable atomic calcium created during the laser ablation process. Additionally, it is important to note that for both $\tilde{A} \rightarrow \tilde{X}$ and $\tilde{B} \rightarrow \tilde{X}$ emission bands, decay to vibrational levels with $v \geqslant 2$ is significantly suppressed to below 0.3%. This rapid decrease in the intensity of off-diagonal vibrational decays should enable experimentally accessible laser cooling and trapping.

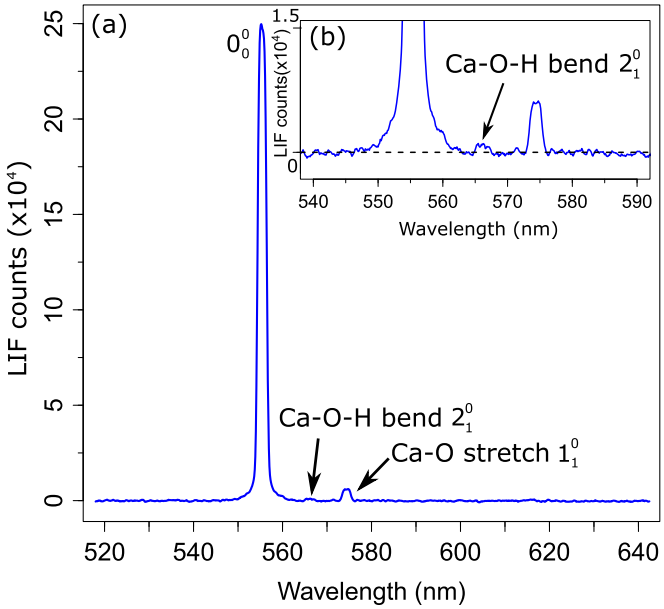

Figure 2. (a) Dispersed LIF data for CaOH excited on the $\tilde{X}$–$\tilde{B}$ electronic transition at 555 nm. (b) Expanded 540–590 nm spectral region indicating a small decay to Ca–O–H bending mode with 1 quanta. $\triangle v_2 = 1$ transitions arising from intensity borrowing due to spin–orbit vibronic interaction has been previously observed in the SrOH spectrum [34].

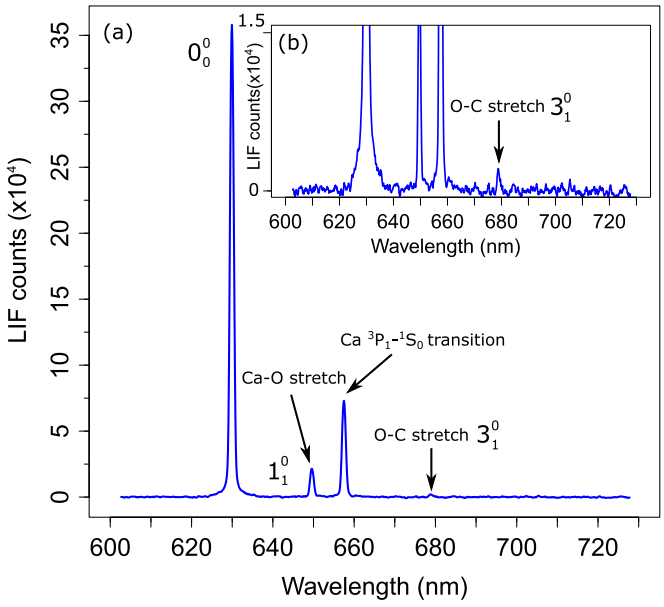

Figure 3. Measurement of the $CaOCH_3$ vibrational branching in the $\tilde{X}$–$\tilde{A}$ electronic system following excitation on the $P_1(N'' = 1)$, $K'' = 1 \rightarrow K' = 0$ transition at 15 886.18 cm^{-1}. Like in the CaOH data, there is a residual signal at 657 nm coming from the spontaneous emission on the intercombination $^3P_1 \rightarrow ^1S_0$ line of metastable calcium atoms. Plot (a) shows that the dominant off-diagonal decay is to the excited Ca–O stretching vibration with one quanta. Plot (b) demonstrates a small peak at 679 nm due to the decay into the excited totally-symmetric vibrational mode composed of O–C and C–H stretching vibrational motions.

3.2. $CaOCH_3$ measurements

The presence of $K \neq 0$ states for nonlinear molecules requires additional considerations for achieving effective photon cycling beyond those examined previously for diatomic and linear polyatomic molecules. Reference [21] outlined how to use $K'' = 1 \rightarrow K' = 0$ transition for the perpendicular $\tilde{X}$–$\tilde{A}$ transition and $K'' = 0 \rightarrow K' = 0$ transition for the parallel $\tilde{X}$–$\tilde{B}$ to achieve rotationally closed excitations. Figures 1 and 3 provide a comparison of the DLIF for CaOH and $CaOCH_3$. Both of the molecules were excited on the $\tilde{X}$–$\tilde{A}$ electronic transitions around 630nm and in a rotationally resolved manner to $J' = 1/2$ state. As can be clearly seen from the data presented, both CaOH and $CaOCH_3$ have a very small number of vibrational decay channels despite significantly increased structural complexity in going from a triatomic to a hexatomic molecule. While

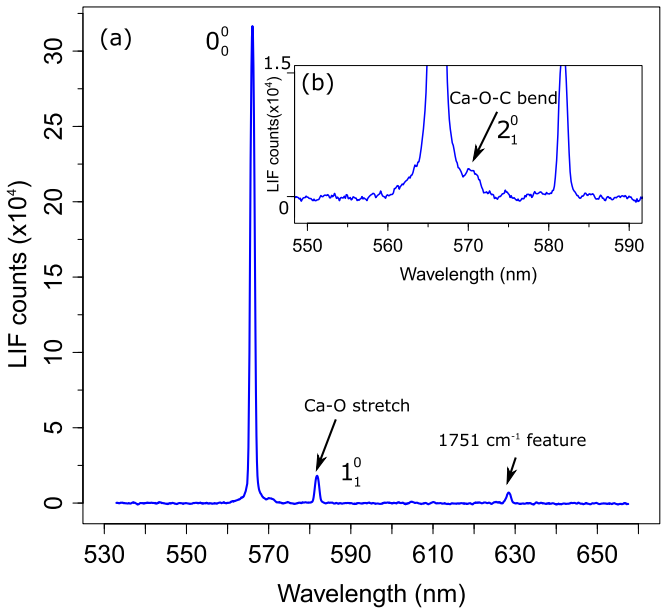

Figure 4. Dispersed laser-induced fluorescence data for $CaOCH_3$ excited on the $\tilde{X}$–$\tilde{B}$ electronic transition at 566 nm using $P_1(N'' = 1)$, $K'' = 0 \rightarrow K' = 0$ branch at 17 682.20 cm^{-1}. (a) Besides the dominant decay to the Ca–O stretching mode, an additional unexpected feature around 1750 cm^{-1} is observed. (b) Lineshape asymmetry on the main peak indicated a $\Delta l \neq 0$ decay to the Ca–O–C bending mode with one unit of vibrational angular momentum l.

$CaOCH_3$ has eight distinct vibrational modes (4 of a_1 symmetry and 4 degenerate pairs of e symmetry), only two are optically active at the three part per thousand level as seen in the figure. Our measurements, performed on a cold molecular beam with a narrow-band dye laser exciting only the rotational level suitable for laser cooling, confirm that even nonlinear CaOR molecules behave effectively like triatomics, showing great promise for laser cooling and trapping.

In order to account for possible systematic effects associated with multiple-photon cycling in our measurements, we have also used excitation to the upper SO component of the $\tilde{A}$ state ($^2\Pi_{3/2}$ for CaOH and $^2E_{3/2}$ for $CaOCH_3$) which does not support rotationally-closed excitations. For all measurements performed, we did not add any additional laser sidebands, thus addressing only a single spin-rotation component. In the presence of optical saturation of the transitions where more than one photon is scattered per single molecule, we anticipate to see $\approx\frac{3}{5}$ less signal in the 0_0^0 emission band when using a non-rotationally closed transition (e.g. R or Q branch). However, for both molecules the measured branching ratios for excitation to either the lower or the upper SO component of the $\tilde{A}$ state are essentially consistent with each other (see tables 5 and 6), providing strong evidence that the measured branch intensities are dominated by the actual FCF values and setting an upper limit on the associated systematic error of 1%. In order to confirm our measurements for the $\tilde{X} \rightarrow \tilde{B}$ transitions we used R-type branch to excite molecules in rotational levels $N'' > 1$, thus preventing optical cycling. Additional data for such measurements is provided in the appendix.

We have also used dispersed LIF to explore the possibility of using the $\tilde{X}$–$\tilde{B}$ electronic transition in $CaOCH_3$ around 566 nm for laser cooling. Figure 4 shows the DLIF results indicating two additional features not present in the $\tilde{A} \rightarrow \tilde{X}$ emission spectrum: (i) emission to 1 quanta of the Ca–O–C bending mode and (ii) a new feature around 1750 cm^{-1} away from the excitation band. Since $\tilde{B}$ is the second excited electronic level, there is a possibility of mixing with the excited vibrational levels of the $\tilde{A}$ state. The proposed intensity borrowing mechanism is shown in figure 5, indicating the resulting decays nominally forbidden by the symmetry arguments. As clearly seen in the data presented in figure 4, a relatively strong emission to the band offset by 1751 cm^{-1} from the diagonal vibronic transition is observed in the $\tilde{B} \rightarrow \tilde{X}$ decay of $CaOCH_3$, making laser cooling on this electronic transition more challenging compared to $\tilde{X} \rightarrow \tilde{A}^2E_{1/2}$.

Any nonlinear molecule (e.g. $CaOCH_3$) in an orbitally degenerate electronic state (e.g. ^2E state) will always distort in a way such as to lower the symmetry and remove degeneracy. This so-called Jahn–Teller effect (JTE) nullifies the $\Delta v_i = \pm 2, \pm 4, \ldots$ selection rule for non-symmetric vibrations in electronic transitions [50]. JTE in the $\tilde{A}$ electronic state as well as near-degeneracy between the excited combination band in the $\tilde{A}$ state and the ground vibrational level of the $\tilde{B}$ electronic state lead to Born–Oppenheimer approximation breakdown. Since the eigenstates of the new Hamiltonian are a mixture of the unperturbed eigenstates of the $\tilde{B}(000)$ and $\tilde{A}(111)$ levels, forbidden decays are observed in the emission spectrum. The appearance of the pseudo-JTE in the presence of accidentally near-degenerate states (as depicted in figure 5) is carefully described in [37]. The

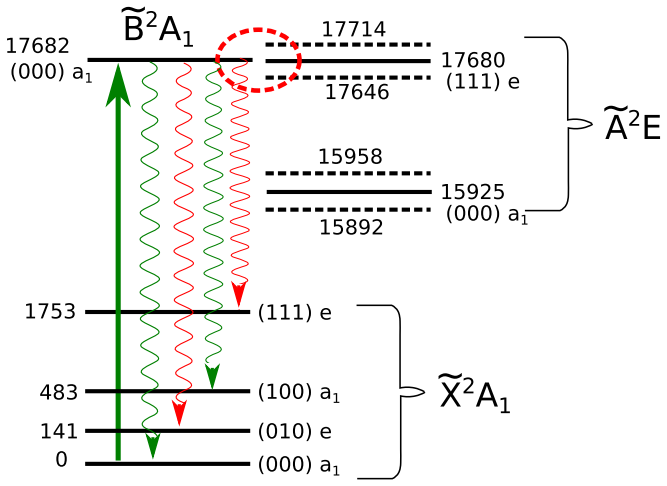

Figure 5. A proposed mechanism of vibronic coupling in $CaOCH_3$ leading to symmetry-forbidden vibrational emissions. By analogy with CaOH, triatomic notation is used for annotating the vibrational modes: ($v_1$00)=Ca–O stretch, (0$v_2$0)=Ca–O–C bend, and (00v_3)=O–C stretch. Red arrows indicate symmetry-forbidden decays allowed by the vibronic mixing between $\tilde{B}(000)$ and $\tilde{A}(111)$. Dashed energy levels indicate the effects of the spin–orbit splitting in the $\tilde{A}$ state. The energies of the vibronic levels are specified in wavenumbers (cm^{-1}).

Table 1. Calculated and measured normal vibrational modes (in units of cm^{-1}) for CaOH. TI and TD stand for time-independent and time-dependent density functional theory calculations, respectively. For doubly-degenerate bending vibrational modes (Π symmetry), the two specified frequencies are for individual A'/A'' states.

State	Mode (symmetry)	TI	TD	Measured [58]	[22]	Combined [References]
$\tilde{X}$	Bend (Π)	356.72	344.89/345.29	352.93	411/408	347.6 [36]
$\tilde{X}$	Ca–O stretch (Σ)	625.22	603.84	609.02	622	612.1 [36]
$\tilde{X}$	O–H stretch (Σ)	3816.28	3819.96	3778	4276	3873.9 [36]
$\tilde{A}$	Bend (Π)	368.41	370.37/371.13	361.36	402/386	349.7/389.8 [57]
$\tilde{A}$	Ca–O stretch (Σ)	625.18	603.84	630.68	646	622.2 [57]
$\tilde{A}$	O–H stretch (Σ)	3816.06	3819.96	—	4279	3989.5 [57]

perturbing operator of the polynomial form in the normal coordinate Q_i about the molecular configuration Q_0 [37]

$$H' = \left(\frac{\partial H}{\partial Q_i}\right)_{Q_0} Q_i + \frac{1}{2}\left(\frac{\partial^2 H}{\partial Q_i^2}\right)_{Q_0} Q_i^2 + \ldots \tag{5}$$

is responsible for mixing of the zeroth-order Born–Oppenheimer vibrational and electronic wavefunctions. Careful theoretical understanding of vibronic coupling in the excited $\tilde{B}$ state is currently in progress and beyond the scope of the present paper.

4. Comparison with theoretical predictions

CaOH three-dimensional potential energy surfaces have been previously mapped out using *ab initio* calculations for both the ground [36] as well as excited electronic states [57]. While table 1 provides a comparison between such *ab initio* results from different studies, we further focus our comparison on the calculations performed by Isaev and Berger [22] since, to our knowledge, they provide the only previous study of CaOH FCFs relevant to laser cooling prospects. Even though there are no previous *ab initio* calculations of FCFs for $CaOCH_3$, the use of isotopically substituted methoxy groups has allowed accurate experimental determination of the radical's geometry in both $\tilde{X}$ and $\tilde{A}$ states [45].

Because of the highly diagonal FCF matrices for both CaOH and $CaOCH_3$ molecules, only a few excited vibrational modes were present in our DLIF data as seen in figures 1–4. Other than the unexpected peak seen in the 1751 nm overtone band for the $\tilde{B} \rightarrow \tilde{X}$ emission, the frequencies of other vibrational modes have been previously measured and tabulated which allowed for unambiguous vibrational character assignment. Theoretical analysis of the multidimensional FCFs for all vibrational modes—including those not observed in the experiment—depends on the frequencies of the corresponding vibrational motions. We therefore initialized

Table 2. Calculated and measured normal vibrational modes (in units of cm^{-1}) for the $\tilde{X}$ electronic state of $CaOCH_3$.

State	Mode (symmetry)	TI	TD	Measured [60]
$\tilde{X}$	Ca–O–C bend (e)	138.59/140.51	133.11/142.09	144 ± 5
$\tilde{X}$	Ca–O stretch (a_1)	482.90	472.09	488 ± 5
$\tilde{X}$	Sym. CH_3 bend and C–O stretch (a_1)	1132.20	945.19	1156 ± 5
$\tilde{X}$	Asymmetric combination (e)	1134.30/1134.61	1109.93/1120.49	—
$\tilde{X}$	Sym. CH_3 bend and C–O stretch (a_1)	1425.76	1385.36	—
$\tilde{X}$	Asymmetric combination (e)	1444.06/1444.42	1425.37/1434.73	—
$\tilde{X}$	Sym. CH_3 stretch (a_1)	2879.18	2886.36	—
$\tilde{X}$	Asymmetric stretch (e)	2922.11/2922.61	2933.60/2933.75	—

Table 3. Calculated and measured normal vibrational modes (in units of cm^{-1}) for the $\tilde{A}$ electronic state of $CaOCH_3$.

State	Mode (symmetry)	TI	TD	Measured [60]
$\tilde{A}$	Ca–O–C bend (e)	141.43/141.54	129.76/141.42	145 ± 5
$\tilde{A}$	Ca–O stretch (a_1)	482.66	472.13	501.48
$\tilde{A}$	Sym. CH_3 bend and C–O stretch (a_1)	1132.24	1119.84	1140 ± 5
$\tilde{A}$	Asymmetric combination (e)	1134.54/1134.62	1206.80/1269.47	—
$\tilde{A}$	Sym. CH_3 bend and C–O stretch (a_1)	1425.48	1 425.10	—
$\tilde{A}$	Asymmetric combination (e)	1 444.08/1444.13	1672.82/1741.32	—
$\tilde{A}$	Sym. CH_3 stretch (a_1)	2879.54	2886.29	—
$\tilde{A}$	Asymmetric stretch (e)	2923.32/2923.36	2931.02/2934.70	—

Table 4. Symmetry coordinates for $MOCH_3$ molecules, listed in an order identical to the basis used for GF calculations. Lower case symmetries (a_1, e) correspond to the irreducible representations of the C_{3v} point group. Coordinates are labeled for the normal modes to which they roughly correspond.

	Coordinate	Symmetry
1	CH_3 symmetric stretch	a_1
2	CH_3 symmetric bend	a_1
3	C–O stretch	a_1
4	M–O stretch	a_1
5	CH_3 asymmetric stretch	e
6	CH_3 asymmetric bend	e
7	O–CH_3 wag	e
8	M–O–C bend	e

our calculations with *ab initio* molecular geometries and vibrational frequencies using the ORCA quantum chemistry program, which is discussed in [59]. Tables 1–3 provide a summary of the calculated normal vibrational modes for CaOH and $CaOCH_3$. We observe excellent agreement between our ORCA calculations with previous *ab initio* calculations for CaOH by Isaev and Berger [22] as well as previously experimentally determined values for the vibrational normal modes. In the case of $MOCH_3$ molecules, there are 12 normal modes, 4 of a_1 symmetry and 4 degenerate pairs of e_1 symmetry. Thus, while there are 12 internal coordinates, we reduced the problem to 8 symmetry coordinates listed in table 4.

The details of the numerical computation of CaOH and $CaOCH_3$ FCFs are described in the appendix. The VBRs were computed by weighting each FCF by the cube of the transition frequency from the vibrationless excited electronic state to the vibrational state in the ground electronic state and normalizing. Results of these calculations are shown in tables 5 and 6. We obtain excellent agreement between the measured and calculated VBRs for CaOH and a reasonable agreement for a more complex $CaOCH_3$ molecule. Incorporating possible couplings between different vibrational modes as well as inclusion of the anharmonic terms in the vibrational potential could resolve the slight discrepancy between the measured and predicted VBRs for $CaOCH_3$. Notice that our theoretical predictions for FCFs are much closer to the measured values we have observed compared to the *ab initio* values predicted by Isaev and Berger [22]. By using available experimental vibrational frequencies to determine the force constants as well as incorporating experimentally measured bond lengths and structure into our analysis, we were able to circumvent some of the challenges associated with predictions of FCFs with

Table 5. Summary of the measured and calculated branching ratios for CaOH molecule.

Band	$\lambda_{v',v''}$, nm	Calc. FCFs	[22] FCFs	Calc. VBRs	Obs. VBRs
$0_0^0\tilde{A}^2\Pi_{1/2}$–$\tilde{X}^2\Sigma^+$	626.5	0.9521	0.9213	0.9570	0.957 ± 0.002
$1_1^0\tilde{A}^2\Pi_{1/2}$–$\tilde{X}^2\Sigma^+$	651.0	0.0459	0.0763	0.0410	0.043 ± 0.002
$2_2^0\tilde{A}^2\Pi_{1/2}$–$\tilde{X}^2\Sigma^+$	654.3	3×10^{-4}	—	3×10^{-4}	$3^{+1}_{-2} \times 10^{-3}$
$0_0^0\tilde{A}^2\Pi_{3/2}$–$\tilde{X}^2\Sigma^+$	623.9	0.9521	0.9213	0.959	0.959 ± 0.005
$1_1^0\tilde{A}^2\Pi_{3/2}$–$\tilde{X}^2\Sigma^+$	648.3	0.0459	0.0763	0.041	0.041 ± 0.005
$0_0^0\tilde{B}^2\Sigma^+$–$\tilde{X}^2\Sigma^+$	555.2	0.9711	—	0.9742	0.975 ± 0.001
$1_1^0\tilde{B}^2\Sigma^+$–$\tilde{X}^2\Sigma^+$	574.4	0.0270	—	0.0244	0.022 ± 0.001
$2_1^0\tilde{B}^2\Sigma^+$–$\tilde{X}^2\Sigma^+$	566.2	0	—	0	0.003 ± 0.001

Table 6. Summary of the measured and calculated branching ratios for $CaOCH_3$ molecule.

Band	$\lambda_{v',v''}$, nm	Calc. FCFs	Calc. VBRs	Obs. VBRs
$0_0^0\tilde{A}^2E_{1/2}$–$\tilde{X}^2A_1$	629.9	0.944	0.950	0.931 ± 0.003
$1_1^0\tilde{A}^2E_{1/2}$–$\tilde{X}^2A_1$	649.5	0.050	0.045	0.063 ± 0.003
$3_1^0\tilde{A}^2E_{1/2}$–$\tilde{X}^2A_1$	678.8	0.003	0.002	0.006 ± 0.003
$0_0^0\tilde{A}^2E_{3/2}$–$\tilde{X}^2A_1$	627.1	0.944	0.954	0.945 ± 0.004
$1_1^0\tilde{A}^2E_{3/2}$–$\tilde{X}^2A_1$	646.6	0.050	0.046	0.055 ± 0.004
$0_0^0\tilde{B}^2A_1$–$\tilde{X}^2A_1$	565.9	0.941	0.947	0.910 ± 0.002
$1_1^0\tilde{B}^2A_1$–$\tilde{X}^2A_1$	581.6	0.049	0.045	0.057 ± 0.002
$2_1^0\tilde{B}^2A_1$–$\tilde{X}^2A_1$	570.3	0	0	0.006 ± 0.002
$1_1^0 2_1^0 3_1^0\tilde{B}^2A_1$–$\tilde{X}^2A_1$	628.2	0	0	0.026 ± 0.002

sufficient accuracy for designing a molecular laser cooling scheme [61]. As seen in table 5, purely *ab initio* calculations for even triatomic FCFs can potentially underestimate the feasibility of direct laser cooling, while calculations relying on molecular parameters extracted from previous spectroscopic data can provide a more accurate guide to developing a successful laser cooling experiment for a new molecule with desired properties (e.g. new physics sensitivity [62]).

5. Laser cooling and trapping prospects

Our experimental measurements and theoretical calculations confirm the possibility of achieving direct laser cooling for CaOH and $CaOCH_3$ with a few repumping lasers. Furthermore, our measurements provide the quantitative guidance to choosing the most experimentally efficient route to identifying the main cooling and all the repumping transition bands. Using the measured values for the branching ratios, we have determined the optimal laser cooling schemes for CaOH and $CaOCH_3$ depicted in figures 6 and 7, respectively. Because of the relatively light mass, CaOH can be slowed down to a complete stop from 100 m s^{-1} CBGB using only 9000 photons which can be obtained with three repumping lasers indicated. Thus, the technical complexity of laser slowing CaOH is comparable to experiments with diatomic molecules SrF and CaF.

While additional structural complexity for $CaOCH_3$ results in less diagonal FCFs, with the repumping scheme in figure 7 and assuming $\sim 10^9$ molecules in a single rovibrational quantum state at 100 m s^{-1}, one can obtain between 10^4 and 10^7 slowed molecules in the trapping region, assuming 1 part per 1000 or 1 part per 3000 loss probability to unaddressed vibrational levels.

6. Beyond symmetric top molecules

Because of the strongly ionic nature of the Ca–O bond in CaOR molecules, the electronic transitions involve non-bonding Ca^+ orbitals perturbed by an RO^- ligand even for asymmetric rotor molecules (ARMs). Since the Ca–O–C bond angle remains 180°, the local symmetry near the calcium metal is linear and therefore many characteristics of electronic transitions carry over from linear CaOH to more complex CaOR symmetric top and asymmetric rotor radicals [35, 63]. For example, there is 'SO' splitting of about the same size, and the electronic orbital angular momentum remains essentially unquenched. However, the symmetry reduction in going from $C_{\infty v}$ (CaOH) and C_{3v} ($CaOCH_3$) to molecules with lower symmetry properties like C_S and no symmetry has potential to impact the VBRs in a significant manner. For linear ($C_{\infty v}$) and symmetric top (C_{3v}) molecules, Ca–O–C bending vibrations have π or e symmetry, correspondingly, and therefore only $\Delta v = \pm 2, \pm 4, \ldots$

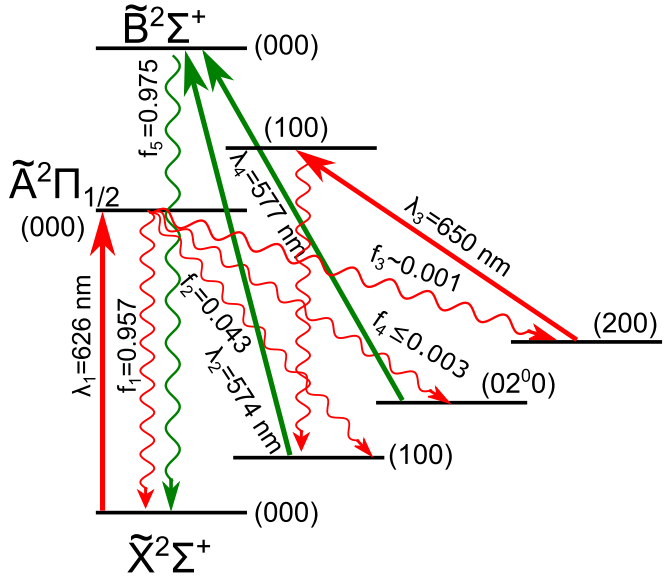

Figure 6. Proposed laser cooling and trapping scheme for CaOH based on the experimental results.

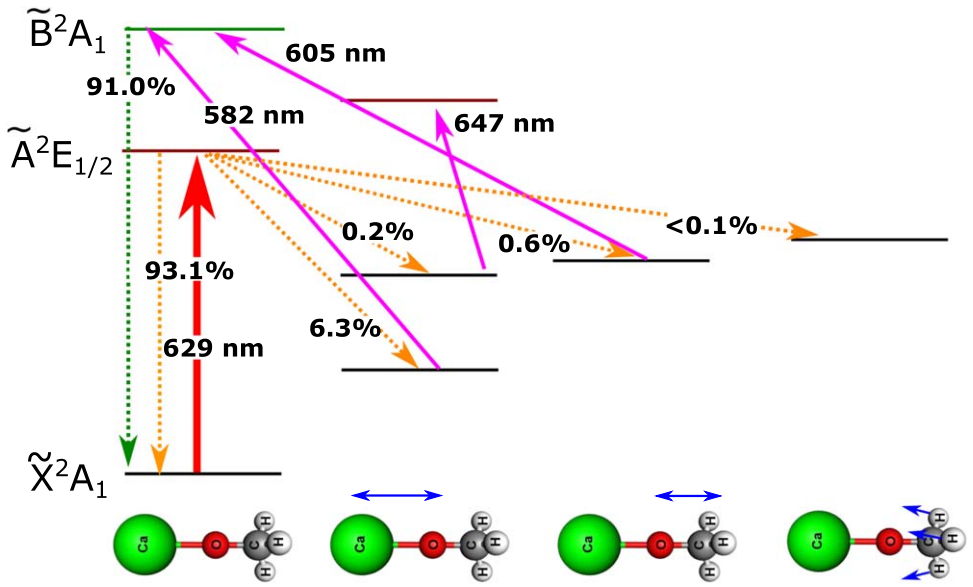

Figure 7. Measured vibrational branching ratios for $CaOCH_3$ along with proposed laser cooling and repumping scheme. The dominant character of the appropriate vibrational mode is indicated.

branches appear in the electronic decays under the Born–Oppenheimer approximation[6]. Such a bending mode becomes non-degenerate for molecules with lower symmetries than C_{3v}, therefore leading to allowed decays of comparable intensity to both one quanta in the Ca–O stretching and Ca–O–C bending modes as has been previously observed for calcium monoalkoxides [35]. While this presents a technical challenge, requiring an additional laser for repumping lost molecules from such a decay channel, it does not pose a fundamental threat to achieving photon cycling in ARMs like $CaOC_2H_5$ or $CaOCH_2CH_3$.

Depending on the orientation of the transition dipole moment relative to the principal axes of the molecule, vibrational and electronic spectra of ARMs are characterized as *a*-type, *b*-type or *c*-type transitions with the selection rules [50]:

[6] Weak forbidden vibronic transitions have been observed for CaOH [64] and SrOH [34] enabled by SO interaction and Renner–Teller coupling. For a detailed description and estimation of the magnitude of the associated SO vibronic coupling resulting in the $\tilde{A}^2\Pi$ 000(Π) ~ $\tilde{B}^2\Sigma^+$ 010(Π) mixing we refer the reader to [37, 65].

- a-type bands: $\triangle K_a = 0$, $\triangle K_c = \pm 1$ and $\triangle J = 0, \pm 1$, except for $K_a' = 0 \leftarrow K_a'' = 0$ for which $\triangle J = \pm 1$
- b-type bands: $\triangle K_a = \pm 1$, $\triangle K_c = \pm 1$ and $\triangle J = 0, \pm 1$
- c-type bands: $\triangle K_c = 0$, $\triangle K_a = \pm 1$ and $\triangle J = 0, \pm 1$, except for $K_c' = 0 \leftarrow K_c'' = 0$ for which $\triangle J = \pm 1$.

Therefore, as can be seen from the selection rules above, for near-oblate or near-prolate ARMs, the overall structure of the emission bands resembles that of parallel or perpendicular transitions for STMs. Choosing either a-type or c-type transitions and driving either $K_c'' = 1 \rightarrow K_c' = 0$ or $K_a'' = 1 \rightarrow K_a' = 0$, correspondingly will resemble optical cycling transitions for STMs as described above. Additionally, using quantum states such as $K_a'' = 0$ or $K_c'' = 0$ for a-type and c-type transitions, correspondingly, will restrict J selection rules to $\triangle J = \pm 1$ only (similarly to $\triangle N = \pm 1$ transitions used for laser cooling diatomic and linear molecules). Thus, while reduced symmetry for ARMs leads to novel challenges in repumping vibrational levels, carefully chosen rotational transitions can significantly limit (or even eliminate) rotational branching. As a first step in achieving photon cycling with ARMs, it is necessary to perform high resolution spectroscopy of the relevant electronic transitions and identify suitable bands for achieving optical cycling. While we have already completed such work for $CaOCH_3$ as described above, similar spectroscopy on more complex CaOR radicals (e.g. $CaOCH_2CH_3$) can be performed in the future. A natural chiral candidate for laser cooling is a chiral analog of calcium monomethoxide, CaOCHDT. A recent theoretical and experimental work by Liu and coworkers [66] on calcium ethoxide ($CaOC_2H_5$) confirms that Ca–O stretching mode is the dominant vibrational loss channel for this molecule and indicates its potential suitability for optical cycling and laser cooling using a scheme outlined here for ARMs.

7. Conclusions and future directions

While the high density of vibronic states for complex polyatomic molecules can potentially inhibit photon cycling using the $\tilde{X}$–$\tilde{B}$ electronic transitions, our measurements provide a strong case that using the lowest excited electronic level ($\tilde{A}$) will enable photon cycling and laser cooling despite the presence of SO and Jahn–Teller interactions. In addition to precise measurements of the VBRs for both $\tilde{X}$–$\tilde{A}$ and $\tilde{X}$–$\tilde{B}$ electronic excitations, we have also performed theoretical calculations that agree quite well for the $\tilde{X}$–$\tilde{A}$ band, where harmonic oscillator approximation remains valid for calculating the multidimensional FCFs. Using the analytical integral expressions presented by Sharp and Rosenstock [67], we have calculated the relevant FCFs using previously available experimental data for geometries, vibrational frequencies, and corresponding force fields. The presence of strong optically accessible electronic transitions, as well as ability to scatter multiple photons from a single molecule, opens the possibility for internal state molecular manipulation and control of the molecular motion in the laboratory frame. While radiative force slowing and cooling requires multiple thousands of repeated absorption-emission cycles [68], Sisyphus cooling processes as well stimulated emission slowing methods can provide significant gains even with a limited number of optical cycles [69, 70]. Stimulated optical forces arising from polychromatic light beams [71, 72] might be especially effective for manipulating MOR molecules with reduced symmetries and increased complexity where scattering tens of thousands of photons would require a large number of vibrational repumping lasers. Additionally, rapid optical cycling of even tens of photons can significantly improve the rate of opto-electrical cooling methods for STMs and ARMs, which have so far relied on using vibrational transitions with long lifetimes and therefore low scattering rates [73, 74].

Laser cooled polyatomic molecules provide an ideal starting point for producing ultracold fundamental radicals of chemical interest like OH, CH_3 and OCH_3. While a dedicated theoretical exploration is necessary for identifying the exact route for efficient photodissociation of polyatomic molecules into underlying constituents with minimal energy released, this approach seems feasible with the use of the STIRAP, which is the reverse of the process employed for forming ultracold diatomic molecules from ultracold alkali atoms [75]. Release of as little as 100 nK of additional kinetic energy into the motion of dissociation products has been achieved with ultracold Sr_2 molecules [76], and an efficient pathway for SrOH zero-kinetic-energy dissociation is currently being developed using *ab initio* molecular potentials [77]. Moreover, modern theoretical approaches to molecular quantum scattering calculations are reaching the regime of larger polyatomic molecules [78] and, therefore, experimental results on collisions would play a crucial role in further developing the field.

Furthermore, our measurements indicate the possibility of multiple photon cycling for other polyatomic species including polyatomic molecular ions. Internal state cooling and control of polyatomic molecular ions can significantly benefit from laser-induced optical cycling. Polyatomic molecular ions $ScOH^+$, YOH^+, as well as $ScOCH_3^+$ and $YOCH_3^+$, are isoelectronic to the corresponding calcium and strontium compounds [79, 80] and should be highly suitable for direct optical manipulation and internal state cooling using methods previously demonstrated with diatomic ions [81]. A few particularly interesting candidates to consider are $AcOH^+$ and $AcOCH_3^+$, which should be similar in electronic structure to RaOH and $RaOCH_3$ and are sensitive

to new physics beyond the standard model [22], but with a significantly longer half-life of the actinium-227 nucleus compared to radium-227 [82].

Another interesting class of molecules to explore is mixed hypermettalic neutral and ionic oxides of the MOM′ type, where M and M′ refer to two different metal elements. Recently, quantum state controlled synthesis of $BaOCa^+$ has been demonstrated [83] and theoretical work on neutral MOM (same metal) molecules has been performed motivated by the potential to search for fine structure constant α variation [84]. Neutral polyatomic molecules functionalized with optical cycling centers like Ca or Sr could also enable interesting applications in quantum sciences [85, 86].

Acknowledgments

The work at Harvard has been supported by the grants from AFOSR and NSF while the work at ASU has been supported by the HSF grant #2018-0681. We would like to thank L Baum and B Augenbraun for insightful discussions. While preparing this manuscript we have learned of another recent work on dispersed LIF of $CaOCH_3$ [87]. However, the details of the measurement method, analysis and resulting conclusions are vastly distinct.

Appendix

A.1. Optimized geometry

In tables A1 and A2 we provide a comparison between the measured and calculated geometries for CaOH and $CaOCH_3$ in the ground and excited electronic states.

A.2. Details of FCF calculations

To compute the FCFs for CaOH and $CaOCH_3$, we used Wilson's GF matrix method and the Sharp–Rosenstock expansion of the FC overlap integral using a harmonic potential. In depth discussion and derivation of these methods are extensively addressed elsewhere [67, 89, 90]. Importantly, the Sharp–Rosenstock expansion depends on the vibrational coordinates of the initial and final states, denoted $\mathbf{Q}'$ and $\mathbf{Q}$ respectively. The relationship between these two coordinate systems is:

$$\mathbf{Q}' = \mathbf{J}\mathbf{Q} + \mathbf{K}, \tag{6}$$

where $\mathbf{K}$ is the difference between the equilibrium geometry of the two states in terms of the initial vibrational coordinates, while $\mathbf{J}$ accounts for coordinate mixing, also known as the Duchinsky effect.

Table A1. Optimized geometry for CaOH.

State	Coordinate	TI	TD	Measured [88]	[22]
$\tilde{X}$	Ca–O	1.9698	1.9656	1.9746	2.0038
$\tilde{X}$	O–H	0.9644	0.964 60	0.9562	0.9333
$\tilde{X}$	∠Ca–O–H	180.00	180.00	180.00	179.97
$\tilde{A}$	Ca–O	1.9698	1.9652	1.9532	1.9769
$\tilde{A}$	O–H	0.9648	0.9646	0.9572	0.9332
$\tilde{A}$	∠Ca–O–H	180.00	180.00	180.00	179.97

Table A2. Optimized geometry for $CaOCH_3$.

State	Coordinate	TI	TD	Measured [45]
$\tilde{X}$	Ca–O	1.9726	1.9636	1.962 ± 0.004
$\tilde{X}$	O-C	1.3989	1.4011	1.411 ± 0.007
$\tilde{X}$	C–H	1.1069	1.1062	1.0937[a]
$\tilde{X}$	∠O–C–H	111.545	111.3	111.3 ± 0.2
$\tilde{A}$	Ca–O	1.972 75	1.9636	1.941 93
$\tilde{A}$	O–C	1.3989	1.401	1.4106
$\tilde{A}$	C–H	1.1068	1.1061	1.0923
$\tilde{A}$	∠O–C–H	111.545	111.3	111.0004[b]

[a] Using methanol tabulation.

[b] Calculated from the available data for the H–C–H angle.

Wilson's GF matrix method [91] is the extension of eigenvalue vibration problems to molecular vibrations, and can be used to find the relationship between **Q** and **Q**′. For an N-atom molecule, we define a set of $3N - 6$ internal coordinates $\{S_t\}$ transformed by $3N$ coefficients B_{ti} from the set of $3N$ Cartesian components $\{\xi_i\}$[7]

$$S_t = \sum_{i=1}^{3N} B_{ti}\xi_i \qquad t = 1, 2, 3 ..., 3N - 6. \tag{7}$$

For convenience, the internal coordinates are often rewritten as N vectors $\mathbf{s}_{t\alpha} = (B_{ti}, B_{ti+1}, B_{ti+2})$ for each atom given fixed $t \in [1, 3N - 6]$. The elements of the **G** (geometry) matrix are derived from mass-weighting the summed scalar product of each of the $3N - 6$ internal coordinates over all atoms, while the **F** (force) matrix elements are derived using a harmonic approximation—each element of the **F** matrix is the second derivative of the potential energy surface with respect to the internal coordinates.

$$G_{tt'} = \sum_{i=1}^{3N} \frac{1}{m_\alpha} B_{ti}B_{t'i} = \sum_{\alpha=1}^{N} \frac{1}{m_\alpha} \mathbf{s}_{t\alpha} \cdot \mathbf{s}_{t'\alpha} \qquad F_{tt'} = \frac{\partial^2 V}{\partial S_t \partial S_{t'}} \tag{8}$$

From the **G** matrix, it is possible to derive the kinetic energy, and from the **F** matrix it is possible to derive the potential energy.

$$2T = \sum_{tt'} (G^{-1}_{tt'})\dot{S}_t\dot{S}_{t'} \qquad 2V = \sum_{tt'} F_{tt'}S_tS_{t'}. \tag{9}$$

Writing the Lagrangian of the system, we end up with a determinant problem:

$$|\mathbf{F} - \mathbf{G}^{-1}\lambda| = \begin{vmatrix} F_{11} - (G^{-1})_{11}\lambda & \cdots & F_{1n} - (G^{-1})_{1n}\lambda \\ F_{21} - (G^{-1})_{21}\lambda & \cdots & F_{2n} - (G^{-1})_{2n}\lambda \\ \vdots & \vdots & \vdots \\ F_{n1} - (G^{-1})_{n1}\lambda & \cdots & F_{nn} - (G^{-1})_{nn}\lambda \end{vmatrix} = 0, \tag{10}$$

where $\lambda = 4\pi^2\nu^2$ and ν is the frequency of a molecular vibration. Multiplying by the determinant of **G**, we get a diagonalization problem: $|\mathbf{G}||\mathbf{F} - \mathbf{G}^{-1}\lambda| = |\mathbf{GF} - \lambda\mathbb{I}| = 0$, where the corresponding eigenvectors are the vibrations (normal modes) in terms of the internal coordinates. Thus, the linear transformation **L** formed by the eigenvectors maps from vibrational normal mode coordinates to internal coordinates. By repeating the GF analysis for the initial and final electronic states, we end up with **L** matrices for both states, and thus can define **Q** and **Q**′.

Specifically, **J** is defined as the product of the inverse of the initial state **L** matrix and and the final state **L**, while **K** is the transformation of the equilibrium difference in internal coordinates to normal coordinates

$$\mathbf{J} = (\mathbf{L}')^{-1}\mathbf{L} \qquad \mathbf{K} = (\mathbf{L}')^{-1}(\mathbf{R}_{\mathrm{eq}} - \mathbf{R}_{\mathrm{eq}}'). \tag{11}$$

Due to vibrational degeneracies, it will often be preferable to reduce the dimensions of the GF problem by concatenating the internal coordinates into symmetry coordinates shown in table 4.

To summarize, these Franck–Condon calculations required knowledge of the molecule geometry, vibrational frequencies, and the potential energy surface in the form of harmonic force constants defined over an internal coordinate system. Suitable internal and symmetry coordinate systems were analytically derived using literature on methanol ($HOCH_3$) [92], and the force constants were fit using PGOPHER software to molecular geometry and spectroscopic data [93].

The force constant fitting was initialized by first reducing the dimensionality of the GF problem to a triatomic situation by treating the CH_3 methyl group as a single atom. Given an ordering of the eigenvalues and neglecting off-diagonal **F** matrix interactions, the 3×3 GF eigenvalue problem is completely determined without knowledge of the diagonal matrix terms. We determine the correct ordering by comparing calculated FC values with known measurements and prior theory, initializing the PGOPHER force constant fitting using force values for the M–O stretch, O–CH_3 stretch, and M–O–C bend symmetry coordinates. To prevent misidentification of normal modes with frequencies, we separately fit the force constants for vibrations of different symmetries, which should be completely decoupled in such a way that the **L** matrix is block-diagonal. We then computed the FC overlap integrals using the Sharp–Rosenstock expansion with the matrices **J**, **K**, and **Γ**, a diagonal matrix consisting of i reduced vibrational frequencies $4\pi^2\nu_i/h$, for both the initial and final electronic states. The FCFs were derived by calculating and normalizing the overlap integral for each vibration up to the third quantum number.

A.3. Additional supporting measurements

In this Section we provide additional supporting data in figures 8–10.

[7] Three degrees of freedom are taken up for position, three for rotation. Accordingly, a linear molecule has $3N - 5$ degrees of freedom due to rotational invariance around the primary symmetry axis.

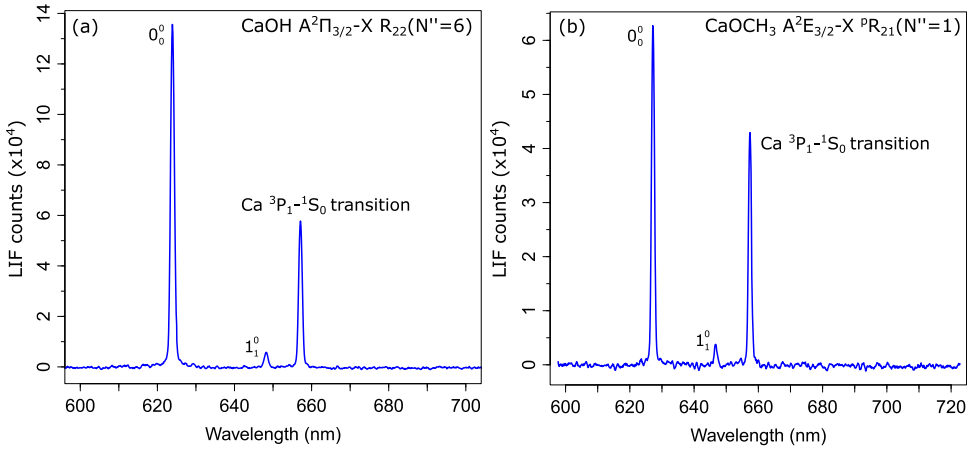

Figure 8. Comparison of DLIF results for CaOH (a) and $CaOCH_3$ (b) excited to the upper spin–orbit component of the $\tilde{X}$–$\tilde{A}$ electronic transition. By using R-branch, we avoid potential systematic error due to accidental optical cycling. As summarized in tables 5 and 6, our measurements are consistent with theoretical predictions and values obtained by exciting the lower spin–orbit

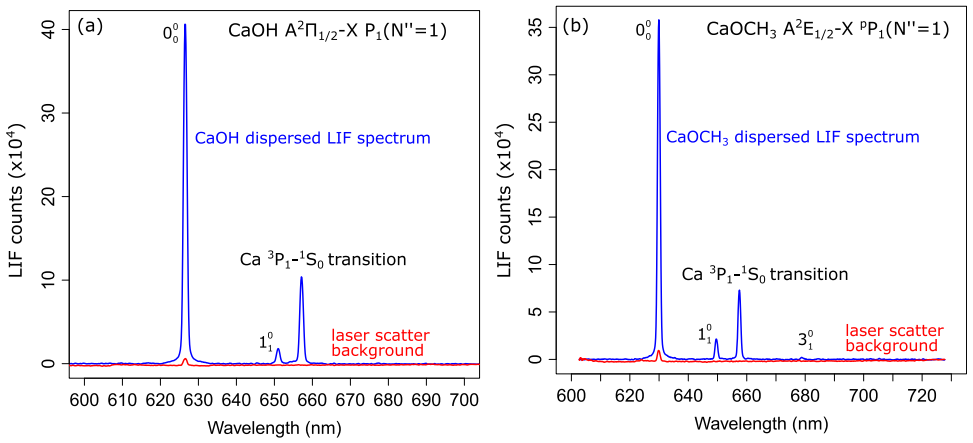

Figure 9. Comparison of DLIF results (blue curves) for CaOH (a) and $CaOCH_3$ (b) excited to the lower spin–orbit component of the $\tilde{X}$–$\tilde{A}$ electronic transition with laser scatter background (red curves) provided for reference. While we have already subtracted laser scatter background from the DLIF data, for both CaOH and $CaOCH_3$ datasets it constituted only a small fraction of the observed signal near the 0_0^0 emission band (as can be seen from the plots here).

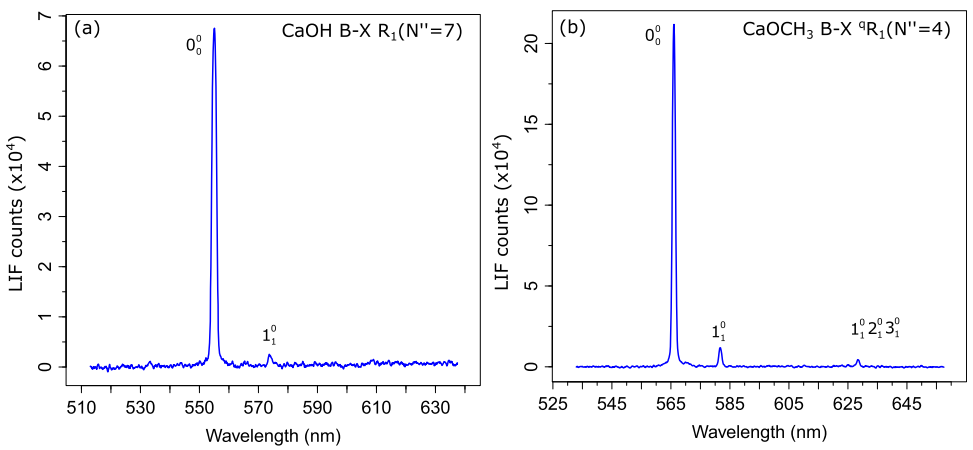

Figure 10. Comparison of DLIF results for CaOH (a) and $CaOCH_3$ (b) excited using R-type branches of the $\tilde{X}$–$\tilde{B}$ electronic transitions. By using a R-branch for $N > 1$ we avoid potential systematic error due to accidental optical cycling, confirming our measurements with the rotationally-closed excitations described in the main text. Observed vibrational decay channels are indicated.

ORCID iDs

Ivan Kozyryev https://orcid.org/0000-0001-5119-6478

References

[1] Krems R V 2008 Cold controlled chemistry *Phys. Chem. Chem. Phys.* **10** 4079–92
[2] Balakrishnan N 2016 Perspective: ultracold molecules and the dawn of cold controlled chemistry *J. Chem. Phys.* **145** 150901
[3] Bohn J L, Rey A M and Ye J 2017 Cold molecules: progress in quantum engineering of chemistry and quantum matter *Science* **357** 1002–10
[4] Narevicius E and Raizen M G 2012 Toward cold chemistry with magnetically decelerated supersonic beams *Chem. Rev.* **112** 4879–89
[5] Lavert-Ofir E, Shagam Y, Henson A B, Gersten S, Kłos J, Żuchowski P S, Narevicius J and Narevicius E 2014 Observation of the isotope effect in sub-kelvin reactions *Nat. Chem.* **6** 332–5
[6] Shagam Y, Klein A, Skomorowski W, Yun R, Averbukh V, Koch C P and Narevicius E 2015 Molecular hydrogen interacts more strongly when rotationally excited at low temperatures leading to faster reactions *Nat. Chem.* **7** 921
[7] Klein A *et al* 2017 Directly probing anisotropy in atom-molecule collisions through quantum scattering resonances *Nat. Phys.* **13** 35–8
[8] Perreault W E, Mukherjee N and Zare R N 2018 Supersonic beams of mixed gases: a method for studying cold collisions *Chem. Phys.* **514** 150–3
[9] Perreault W E, Mukherjee N and Zare R N 2017 Quantum control of molecular collisions at 1 Kelvin *Science* **358** 356–9
[10] Hutzler N R, Lu H-I and Doyle J M 2012 The buffer gas beam: an intense, cold, and slow source for atoms and molecules *Chem. Rev.* **112** 4803–27
[11] Lemeshko M, Krems R V, Doyle J M and Kais S 2013 Manipulation of molecules with electromagnetic fields *Mol. Phys.* **111** 1648
[12] Jankunas J and Osterwalder A 2015 Cold and controlled molecular beams: production and applications *Annu. Rev. Phys. Chem.* **66** 241–62
[13] Jin D and Ye J 2011 Polar molecules in the quantum regime *Phys. Today* **64** 27
[14] Campbell W C, Tscherbul T V, Lu H-I, Tsikata E, Krems R V and Doyle J M 2009 Mechanism of collisional spin relaxation in $^3\Sigma$ molecules *Phys. Rev. Lett.* **102** 013003
[15] Maussang K, Egorov D, Helton J S, Nguyen S V and Doyle J M 2005 Zeeman relaxation of CaF in low-temperature collisions with helium *Phys. Rev. Lett.* **94** 123002
[16] Shuman E S, Barry J F and Demille D 2010 Laser cooling of a diatomic molecule *Nature* **467** 820–3
[17] Hummon M T, Yeo M, Stuhl B K, Collopy A L, Xia Y and Ye J 2013 2D magneto-optical trapping of diatomic molecules *Phys. Rev. Lett.* **110** 143001
[18] Truppe S, Williams H, Hambach M, Caldwell L, Fitch N, Hinds E, Sauer B and Tarbutt M 2017 Molecules cooled below the Doppler limit *Nat. Phys.* **13** 1173
[19] Anderegg L, Augenbraun B L, Chae E, Hemmerling B, Hutzler N R, Ravi A, Collopy A, Ye J, Ketterle W and Doyle J M 2017 Radio frequency magneto-optical trapping of CaF with high density *Phys. Rev. Lett.* **119** 103201
[20] Anderegg L, Augenbraun B L, Bao Y, Burchesky S, Cheuk L W, Ketterle W and Doyle J M 2018 Laser cooling of optically trapped molecules *Nat. Phys.* **14** 890
[21] Kozyryev I, Baum L, Matsuda K and Doyle J M 2016 Proposal for laser cooling complex polyatomic molecules *ChemPhysChem* **17** 3641–8
[22] Isaev T and Berger R 2016 Polyatomic candidates for cooling of molecules with lasers from simple theoretical concepts *Phys. Rev. Lett.* **116** 063006
[23] Kozyryev I, Baum L, Matsuda K, Augenbraun B L, Anderegg L, Sedlack A and Doyle J M 2017 Sisyphus laser cooling of a polyatomic molecule *Phys. Rev. Lett.* **118** 173201
[24] Herzberg G 1966 *Molecular Spectra and Molecular Structure. Vol 3: Electronic Spectra and Electronic Structure of Polyatomic Molecules* (New York: Van Nostrand, Reinhold)
[25] Wells N and Lane I C 2011 Electronic states and spin-forbidden cooling transitions of AlH and AlF *Phys. Chem. Chem. Phys.* **13** 19018–25
[26] Moore K and Lane I C 2018 Quantitative theoretical analysis of lifetimes and decay rates relevant in laser cooling BaH *J. Quantum Spectrosc. Radiat. Transfer* **211** 96–106
[27] Gao Y and Gao T 2014 Laser cooling of the alkaline-earth-metal monohydrides: insights from an *ab initio* theory study *Phys. Rev.* A **90** 052506
[28] Isaev T, Zaitsevskii A and Eliav E 2017 Laser-coolable polyatomic molecules with heavy nuclei *J. Phys. B: At. Mol. Opt. Phys.* **50** 225101
[29] Hendricks R, Holland D, Truppe S, Sauer B and Tarbutt M 2014 Vibrational branching ratios and hyperfine structure of ^{11}BH and its suitability for laser cooling *Front. Phys.* **2** 51
[30] Smallman I, Wang F, Steimle T, Tarbutt M and Hinds E 2014 Radiative branching ratios for excited states of ^{174}YbF: application to laser cooling *J. Mol. Spectrosc.* **300** 3–6
[31] Zhuang X *et al* 2011 Franck–Condon factors and radiative lifetime of the $A^2\Pi_{1/2}$–$X^2\Sigma^+$ transition of ytterbium monofluoride, YbF *Phys. Chem. Chem. Phys.* **13** 19013–7
[32] Hunter L, Peck S, Greenspon A, Alam S S and DeMille D 2012 Prospects for laser cooling TlF *Phys. Rev.* A **85** 012511
[33] Nguyen D-T, Steimle T C, Kozyryev I, Huang M and McCoy A B 2018 Fluorescence branching ratios and magnetic tuning of the visible spectrum of SrOH *J. Mol. Spectrosc.* **347** 7–18
[34] Brazier C and Bernath P 1985 Laser and fourier transform spectroscopy of the $\tilde{A}^2\Pi$–$\tilde{X}^2\Sigma^+$ transition of SrOH *J. Mol. Spectrosc.* **114** 163–73
[35] Brazier C, Ellingboe L, Kinsey-Nielsen S and Bernath P 1986 Laser spectroscopy of alkaline earth monoalkoxide free radicals *J. Am. Chem. Soc.* **108** 2126–32
[36] Koput J and Peterson K A 2002 *Ab initio* potential energy surface and vibrational-rotational energy levels of $X^2\Sigma^+$ CaOH *J. Phys. Chem.* A **106** 9595–9
[37] Fischer G 1984 *Vibronic Coupling: The Interaction Between the Electronic and Nuclear Motions* vol 9 (New York: Academic)
[38] Salumbides E, Eikema K, Ubachs W, Hollenstein U, Knöckel H and Tiemann E 2006 The hyperfine structure of $^{129}I_2$ and $^{127}I^{129}I$ in the $B^3\Pi_{0_u^+}$–$X^1\Sigma_g^+$ band system *Mol. Phys.* **104** 2641–52
[39] Stuhl B K, Sawyer B C, Wang D and Ye J 2008 Magneto-optical trap for polar molecules *Phys. Rev. Lett.* **101** 243002

[40] Di Rosa M 2004 Laser-cooling molecules *Eur. Phys. J.* D **31** 395–402
[41] Shuman E, Barry J, Glenn D and DeMille D 2009 Radiative force from optical cycling on a diatomic molecule *Phys. Rev. Lett.* **103** 223001
[42] Kozyryev I, Baum L, Matsuda K, Hemmerling B and Doyle J M 2016 Radiation pressure force from optical cycling on a polyatomic molecule *J. Phys. B: At. Mol. Opt. Phys.* **49** 134002
[43] Bernath P and Kinsey-Nielsen S 1984 Dye laser spectroscopy of the $B^2\Sigma^+$–$X^2\Sigma^+$ transition of CaOH *Chem. Phys. Lett.* **105** 663–6
[44] Crozet P, Martin F, Ross A, Linton C, Dick M and Adam A 2002 The A^2E–X^2A_1 system of $CaOCH_3$ *J. Mol. Spectrosc.* **213** 28–34
[45] Crozet P, Ross A, Linton C, Adam A, Hopkins W and Roy R Le 2005 Geometry of the $CaOCH_3$ radical from isotope effects in the $\tilde{A}^2E$–$\tilde{X}^2A_1$ transition *J. Mol. Spectrosc.* **229** 224–30
[46] Whitham C, Beaton S, Ito Y and Brown J 1998 Laser excitation spectroscopy of the $\tilde{B}^2A_1$–$\tilde{X}^2A_1$ Transition of the $CaOCH_3$ Radical *J. Mol. Spectrosc.* **191** 286–94
[47] Bernath P and Brazier C 1985 Spectroscopy of CaOH *Astrophys. J.* **288** 373–6
[48] Steimle T, Fletcher D, Jung K and Scurlock C 1992 A supersonic molecular beam optical Stark study of CaOH and SrOH *J. Chem. Phys.* **96** 2556–64
[49] Namiki K-I C, Robinson J S and Steimle T C 1998 A spectroscopic study of $CaOCH_3$ using the pump/probe microwave and the molecular beam/optical Stark techniques *J. Chem. Phys.* **109** 5283–9
[50] Bernath P F 2005 *Spectra of Atoms and Molecules* 2nd edn (Oxford: Oxford University Press)
[51] Tarbutt M, Sauer B, Hudson J and Hinds E 2013 Design for a fountain of YbF molecules to measure the electron's electric dipole moment *New J. Phys.* **15** 053034
[52] Williams H, Truppe S, Hambach M, Caldwell L, Fitch N, Hinds E, Sauer B and Tarbutt M 2017 Characteristics of a magneto-optical trap of molecules *New J. Phys.* **19** 113035
[53] Wall T, Kanem J, Hudson J, Sauer B, Cho D, Boshier M, Hinds E and Tarbutt M 2008 Lifetime of the A ($v'=0$) state and Franck–Condon factor of the A-X (0-0) transition of CaF measured by the saturation of laser-induced fluorescence *Phys. Rev.* A **78** 062509
[54] Bolman P and Brown J 1973 The Renner–Teller effect and vibronically induced bands in the electronic spectrum of NCO *Chem. Phys. Lett.* **21** 213–6
[55] Brown J 1977 The effective Hamiltonian for the Renner–Teller effect *J. Mol. Spectrosc.* **68** 412–22
[56] Presunka P I and Coxon J A 1994 Laser spectroscopy of the $\tilde{A}^2\Pi$–$\tilde{X}^2\Sigma^+$ transition of SrOH: deperturbation analysis of K-resonance in the $v_2 = 1$ level of the $\tilde{A}^2\Pi$ state *J. Chem. Phys.* **101** 201–22
[57] Taylor C M, Chaudhuri R K and Freed K F 2005 Electronic structure of the calcium monohydroxide radical *J. Chem. Phys.* **122** 044317
[58] Jacox M E 1998 Vibrational and electronic energy levels of polyatomic transient molecules. Supplement A *J. Phys. Chem. Ref. Data* **27** 115–393
[59] Neese F 2012 The ORCA program system *Wiley Interdiscip. Rev.: Comput. Mol. Sci.* **2** 73–8
[60] Jacox M E 2003 Vibrational and electronic energy levels of polyatomic transient molecules. Supplement B *J. Phys. Chem. Ref. Data* **32** 1–441
[61] Isaev T, Hoekstra S and Berger R 2010 Laser-cooled RaF as a promising candidate to measure molecular parity violation *Phys. Rev.* A **82** 052521
[62] Norrgard E B, Barker D S, Eckel S P, Fedchak J A, Klimov N N and Scherschligt J 2018 Nuclear-spin dependent parity violation in optically trapped polyatomic molecules arXiv:1812.00064
[63] Brazier C, Bernath P, Kinsey-Nielsen S and Ellingboe L 1985 Laser spectroscopy of organometallic free radicals *J. Chem. Phys.* **82** 1043–5
[64] Coxon J A, Li M G and Presunka P I 1994 Laser spectroscopy of the $(010)^2\Sigma^{(+)}$, $^2\Sigma^{(-)}$–$(000)^2\Sigma^+$ parallel bands in the $\tilde{A}^2\Pi$-$X^2\Sigma^+$ system of CaOH *J. Mol. Spectrosc.* **164** 118–28
[65] Kozyryev I 2017 Laser cooling and inelastic collisions of the polyatomic radical SrOH *PhD Thesis* Harvard University
[66] Paul A C, Reza M A and Liu J 2016 Dispersed-fluorescence spectroscopy of jet-cooled calcium ethoxide radical ($CaOC_2H_5$) *J. Mol. Spectrosc.* **330** 142–6
[67] Sharp T and Rosenstock H 1964 Franck–Condon factors for polyatomic molecules *J. Chem. Phys.* **41** 3453–63
[68] McCarron D 2018 Laser cooling and trapping molecules *J. Phys. B: At. Mol. Opt. Phys.* **51** 212001
[69] Metcalf H 2017 Colloquium: strong optical forces on atoms in multifrequency light *Rev. Mod. Phys.* **89** 041001
[70] Cashen M, Rivoire O, Romanenko V, Yatsenko L and Metcalf H 2001 Strong optical forces in frequency-modulated light *Phys. Rev.* A **64** 063411
[71] Kozyryev I, Baum L, Aldridge L, Yu P, Eyler E E and Doyle J M 2018 Coherent bichromatic force deflection of molecules *Phys. Rev. Lett.* **120** 063205
[72] Galica S, Aldridge L, McCarron D, Eyler E and Gould P 2018 Deflection of a molecular beam using the bichromatic stimulated force *Phys. Rev.* A **98** 023408
[73] Zeppenfeld M, Englert B G, Glöckner R, Prehn A, Mielenz M, Sommer C, van Buuren L D, Motsch M and Rempe G 2012 Sisyphus cooling of electrically trapped polyatomic molecules *Nature* **491** 570
[74] Prehn A, Ibrügger M, Glöckner R, Rempe G and Zeppenfeld M 2016 Optoelectrical cooling of polar molecules to submillikelvin temperatures *Phys. Rev. Lett.* **116** 063005
[75] Vitanov N V, Rangelov A A, Shore B W and Bergmann K 2017 Stimulated raman adiabatic passage in physics, chemistry, and beyond *Rev. Mod. Phys.* **89** 015006
[76] McDonald M P 2018 High precision optical spectroscopy and quantum state selected photodissociation of ultracold $^{88}Sr_2$ molecules in an optical lattice *Springer Theses* Springer International Publishing
[77] Klos J, Li M, Petrov A and Kotochigova S 2018 Chemistry of laser-coolable polyatomic molecules *Bull. Am. Phys. Soc.*
[78] Huang J, Liu S, Zhang D H and Krems R V 2018 Time-dependent wave packet dynamics calculations of cross sections for ultracold scattering of molecules *Phys. Rev. Lett.* **120** 143401
[79] Huang Y, Hill Y and Freiser B S 1991 Study of the gas-phase chemistry of yttrium-methyl cation YCH^+: σ-bond metathesis and migratory insertion of C-C bonds into the Y^+-methyl bond *J. Am. Chem. Soc.* **113** 840–5
[80] Huang Y, Wise M, Jacobson D and Freiser B 1987 Gas-phase reactions of yttrium and lanthanum ions with alkanes by fourier transform mass spectrometry *Organometallics* **6** 346–54
[81] Lien C-Y, Seck C M, Lin Y-W, Nguyen J H, Tabor D A and Odom B C 2014 Broadband optical cooling of molecular rotors from room temperature to the ground state *Nat. Commun.* **5** 4783
[82] Roberts B, Dzuba V and Flambaum V 2014 Strongly enhanced atomic parity violation due to close levels of opposite parity *Phys. Rev.* A **89** 042509

[83] Puri P, Mills M, Schneider C, Simbotin I, Montgomery J A, Côté R, Suits A G and Hudson E R 2017 Synthesis of mixed hypermetallic oxide $BaOCa^+$ from laser-cooled reagents in an atom-ion hybrid trap *Science* **357** 1370–5
[84] Ostojic B, Jensen P, Schwerdtfeger P and Bunker P 2013 The predicted spectrum and singlet-triplet interaction of the hypermetallic molecule SrOSr *J. Phys. Chem.* A **117** 9370–9
[85] Kozyryev I and Hutzler N R 2017 Precision measurement of time-reversal symmetry violation with laser-cooled polyatomic molecules *Phys. Rev. Lett.* **119** 133002
[86] O'Rourke M J and Hutzler N R 2019 Hypermetallic polar molecules for precision measurements arXiv:1902.10683
[87] Liu J, Miller T A, Sharma K, Reza M A and Paul A C 2018 Alkaline earth monoalkoxide free radicals as candidates for laser cooling of polyatomic molecules *Int. Symp. on Molecular Spectroscopy*
[88] Li M and Coxon J A 1996 Dye laser excitation studies of the $\tilde{A}^2\Pi(100)/(020)$–$\tilde{X}^2\Sigma^+(020)/(000)$ bands of CaOD: analysis of the $\tilde{A}^2\Pi$ (100)~(020) Fermi resonance *J. Chem. Phys.* **104** 4961–77
[89] Wilson E B, Decius J C and Cross P C 1980 *Molecular Vibrations: The Theory of Infrared and Raman Vibrational Spectra* (Chelmsford, MA: Courier Corporation)
[90] Weber J and Hohlneicher G 2003 Franck–Condon factors for polyatomic molecules *Mol. Phys.* **101** 2125–44
[91] Ng C-Y, Baer T and Powis I 1994 *Unimolecular and Bimolecular Ion–Molecule Reaction Dynamics* vol 3 (New York: Wiley)
[92] Zhao S and Ghosh S 1995 Vibrational frequency and force field constant calculation of CH_3OH and its 9 isotopomers by GF matrix method *Int. J. Infrared Millim. Waves* **16** 547–77
[93] Western C M 2017 PGOPHER: a program for simulating rotational, vibrational and electronic spectra *J. Quantum Spectrosc. Radiat. Transfer* **186** 221–42